Journal of Ceramic Processing Research. Vol. 18, No. 2, pp. 127~136 (2017)

J O U R N A L O F
Ceramic Processing Research

Thermomechanical characteristics of HDPE/$CaCO_3$/LDPE-g-MA composites for melt-mixing conditions

Youngjun Ahn[a], Ji Whan Ahn[b] and Choon Han[a,*]

[a]*Department of Chemical Engineering, Kwangwoon University, 20 Gwangun-ro, Nowon-gu, Seoul 139-701, Korea*

[b]*Mineral Resources Research Division, Korea Institute of Geoscience and Mineral Resources, 124 Gwahak-ro, Yuseong-gu, Daejeon 305-350, Korea*

The novel characteristics of high-density polyethylene (HDPE)/calcium carbonate ($CaCO_3$)/maleic anhydride grafted low-density polyethylene (LDPE-g-MA) composites were examined in relation to the reaction temperature and the amount of LDPE-g-MA for melt mixing conditions. HDPE/$CaCO_3$/LDPE-g-MA composites were prepared by melt mixing. The tensile strength of the composites decreased with increase in $CaCO_3$, but thermogravimetric analysis (TGA) revealed that the composites had higher thermal stability than pure HDPE. Differential scanning calorimetry (DSC) analysis showed that the crystallinity (X_c) and crystallization entropy (ΔS_c) of the composites decreased with increase in temperature and the amount of LDPE-g-MA. These results were consistent with the activation energy (E_a) derived from the Kissinger method. This study demonstrates that the composites were influenced by the temperature and the amount of LDPE-g-MA. In addition, a certain amount of $CaCO_3$ is expected to act as a stable nucleating agent, which thus accelerates the crystallization rate.

Key words: Hybrid composites, Polymer-matrix composites (PMCs), Thermomechanical properties.

Introduction

Extensive research is being conducted on hybrid materials, which are composites comprised of polymers/inorganic fillers. Thermal plastic polymers continue to be produced, and are widely used across industries. One of the most representative polymers is polyethylene (PE). PE is cheap, has outstanding optical properties, absorbs almost no water, and has excellent resistance to heat sealing, and acids and/or bases [1]. However, the lack of polar groups in PE causes poor surface compatibility, which results in some constraints in the dispersion of inorganic fillers.

Many studies have been performed on inorganic fillers in polymer/inorganic filler composites, such as calcium carbonate ($CaCO_3$) [2-11], clay [12, 13], silica [14, 15], talc [16], and other fillers [17-19]. Compared to pure polymers, these composites have enhanced thermal [3, 20] and mechanical properties [8, 11], due to interfacial interactions between the polymers and inorganic particles. $CaCO_3$ is a good example of inorganic filler. Blends of $CaCO_3$ and polymers are used to improve mechanical and thermal properties for various industrial applications. For the past few decades, the industrial demand for $CaCO_3$ has shown steady increase, thanks to its affordability, availability, diverse shapes, and outstanding physical/chemical properties. As such, it is commonly used in polyolefin composites as filler. However, the poor interfacial adhesion between organic polymers and inorganic fillers weakens the mechanical properties of such composites. Thus, research had focused on improving the interactions between organic polymers and inorganic fillers.

Tanniru et al. [5] showed that adding $CaCO_3$ to high-density polyethylene (HDPE) improved the mechanical and thermal properties, while nucleation remained unaffected. Blending varying amounts of $CaCO_3$ with low-density polyethylene (LDPE) resulted in mechanical and thermal degradation [21]. In $CaCO_3$/LDPE/LLDPE (linear low-density polyethylene) composites, an increase in $CaCO_3$ decreased the melt flow rate [22]. In addition, research on the surface treatment of $CaCO_3$ is being carried out to enhance $CaCO_3$ dispersion and lower the surface energy. Osman et al. [23] examined the influence of LDPE/$CaCO_3$ composites coated with stearic acid (SA). They found that stearic acid increased the modulus and yield stress, but reduced tensile strength and ultimate elongation. Lazzeri et al. [24] investigated the effect of stearic acid coating on HDPE/$CaCO_3$ nano-composites. Compared to uncoated nano-composites, the addition of $CaCO_3$ to SA-coated HDPE led to a decrease in the Young's modulus and yield stress. Research on nano-sized $CaCO_3$ blended with PE is also being carried out [24-28]. Sahebian et al. [25] demonstrated that the mechanical properties of PE/$CaCO_3$ composites became more significant for smaller particle sizes of $CaCO_3$. On the other hand, Martinez-Garcial et al. [29] showed

*Corresponding author:
Tel : +82-2-940-5175
Fax: +82-2-909-0667
E-mail: chan@kw.ac.kr

that high agglomeration occurred with smaller $CaCO_3$ particles due to the larger specific surface area. Composites other than PE and $CaCO_3$ have been actively studied. Wang et al. [30] found that adding SA-coated $CaCO_3$ to polypropylene (PP) enhanced the mechanical properties. Polyvinyl chloride (PVC) with nano-sized $CaCO_3$ had a higher viscosity than pure PVC [31]. Chen et al. [32] showed that adding nano-sized $CaCO_3$ to polybutylene succinate (PBS) improved the thermal stability. This addition also significantly enhanced the storage modulus and loss modulus. Some studies have covered the deformation of isotactic polypropylene (iPP) and $CaCO_3$ [33]. Most research concentrated on the effect of inorganic surface treatment or nano-sized inorganic fillers on the mechanical and thermal properties.

The purpose of this study was to investigate the novel behavior of the structural characteristics, mechanical properties, thermal properties, and non-isothermal crystallization of HDPE/$CaCO_3$/LDPE-g-MA composites in relation to the temperature and amount of LDPE-g-MA. The HDPE/$CaCO_3$/LDPE-g-MA composites were analyzed in terms of their crystal structure, tensile strength, crystallization behavior, thermal stability, and non-isothermal crystallization kinetics and activation energies.

Experimental

Materials

The HDPE/$CaCO_3$/LDPE-g-MA composites were prepared with HDPE by LG Chemical Co. Korea and $CaCO_3$ by Duksan Co. Korea. The LDPE-g-MA [2] prepared and used in this study had the highest grafting degree of 4.88%.

Preparation of the HDPE/$CaCO_3$/LDPE-g-MA compsites

The melt mixing was performed for five minutes at 50 rpm in a Haake mixer (Rheomix 600, Germany) to identify the effect of the reaction temperature (Table 1) and amount of LDPE-g-MA (Table 2) on HDPE/$CaCO_3$/LDPE-g-MA composites. The samples were prepared by compression molding under constant pressure for two minutes at 130 °C using a hot press (Carver, USA). They were then cold pressed between two plates at room temperature for three minutes [2].

Characterization of the HDPE/$CaCO_3$/LDPE-g-MA composites

The tensile strength of the composites was measured using a universal testing machine (UTM, Tiniusolsen, USA) at room temperature in accordance with ASTM D638. All measurements were taken at a head speed of 10 mm/min, and average values were obtained from five repeated tests.

The crystal structure of the HDPE/$CaCO_3$/LDPE-g-MA composites was determined through X-ray diffraction (XRD, Rigaku, Japan) with Cu Kα radiation (λ = 0.154 nm) at room temperature within a 2θ range from 10 to 50 degrees. To verify these findings, the *d*-spacing of HDPE/$CaCO_3$/LDPE-g-MA composites in relation to temperature was calculated using Bragg's law.

$$\lambda = 2d \sin\theta \quad (1)$$

where λ is the wavelength of the incident radiation, d is the interplanar spacing (nm), and θ is the scattering angle. Thermogravimetric analysis (TGA, TGA Q500, USA) was performed to assess the thermal stability of all composites. The samples were heated at 5 °C/min from 25 to 900 °C under a nitrogen atmosphere. To examine the crystallization behavior, non-isothermal crystallization kinetic, and activation energy, differential scanning calorimetry (DSC, DSC Q1000, USA) was carried out at a cooling rate of 5 °C/min from 200 °C to room temperature under a nitrogen atmosphere. The crystallinity of the composite was determined by the following.

$$X_C(\%) = \frac{\Delta H_C}{(1-\omega)\times\Delta H^*}\times 100 \quad (2)$$

where X_C is the crystallinity (%), ΔH_C is the measured melting enthalpy (J/g), ΔH^* is the melting enthalpy of HDPE (293 J/g) [34], and ω is the weight fraction of HDPE of the composites. Conformational change was determined from the crystallization entropy (ΔS_c), as

Table 1. Description in relation to the reaction temperature of the HDPE/$CaCO_3$/LDPE-g-MA composites.

Sample name	Temperature (°C)	Weight ratio (%) of HDPE/$CaCO_3$/ LDPE-g-MA
HCLM1	140	25/58.32/16.68
HCLM2	160	
HCLM3	180	
HCLM4	200	
HCLM5	220	
HCLM6	240	
HCLM7	140	58.32/25/16.68
HCLM8	160	
HCLM9	180	
HCLM10	200	
HCLM11	220	
HCLM12	240	

Table 2. Description in relation to the amount of LDPE-g-MA of the HDPE/$CaCO_3$/LDPE-g-MA composites.

Sample name	Temperature (°C)	Weight ratio (%) of HDPE/$CaCO_3$/ LDPE-g-MA
HCLM1-9	140	27/64/9
HCLM1-23		23/54/23
HCLM7-9		64/27/9
HCLM7-23		54/23/23

shown below [35].

$$\Delta S_c = \frac{\Delta H_c}{T_c} \tag{3}$$

where ΔH_c is the enthalpy of crystallization, and T_c is the crystallization temperature. The relative crystallinity X_T in relation to temperature was calculated by the following equation.

$$X_T = \frac{\int_{T_o}^{T} (dH_c/dT)dT}{\int_{T_o}^{T_f} (dH_c/dT)dT} \tag{4}$$

where T_o and T_f are the onset and finishing temperature of crystallization respectively, and dH_c/dT is the heat flow rate. The crystallization time (t), in relation to temperature was calculated as follows.

$$t = \frac{(T_o - T_c)}{\alpha} \tag{5}$$

where T_o and T_c are the onset and finishing temperature of crystallization respectively, and α is the cooling rate. Furthermore, the Avrami model [36], commonly used in research on the crystallization dynamics of polymers and composites was employed for dynamic isothermal crystallization analysis.

$$ln[-ln(1-X_t)] = Z_t + nlnt \tag{6}$$

where X_t is the relative crystallinity, n is the Avrami exponent, and Z_t is the rate constant in relation to time. To express the non-isothermal crystallization, Jeziorny [37] determined the rate constant (Z_c) by introducing the cooling rate shown in Eq. 7.

$$lnZ_c = \frac{lnZ_t}{\alpha} \tag{7}$$

The Kissinger method [38] was employed to determine the crystallization activation energy (E_a) of pure HDPE and the composites using DSC data.

$$ln\frac{\alpha}{T_c^2} = \frac{E_a}{R}\frac{1}{T_c} \tag{8}$$

where α is the cooling rate, T_c is the crystallization temperature and R is the gas constant.

Results and Discussion

Since the heat received by the composites during melt mixing affects the reduction in molecular weight and thermal degradation, it is considered an important variable. This is because when melt mixing is performed at high temperatures, the mechanical properties of composites deteriorate, due to exposure to unnecessary heat. The mechanical properties also contain important information about the internal structure of the composites [39].

The melt mixing was conducted for five minutes at 50 rpm under various temperatures to examine the effect of reaction temperature. Fig. 1 gives the tensile strength of all composites except HCLM5 and HCLM6. The tensile strength showed a decreasing trend with increasing temperature. This indicates that matrix functions are likely to deteriorate with decrease in the molecular weight of HDPE, which results from thermal degradation when melt mixing is carried out at temperatures higher than the melting point of pure HDPE. The tensile strength of HCLM5 and HCLM6 could not be measured as the samples were easily broken. The samples with relatively higher amounts of HDPE, from HCLM7 to HCLM12, exhibited higher tensile strength than those from HCLM1 to HCLM4. The filler fraction is known to influence the tensile strength of composites as well as interactions between the filler and the polymer matrix. The tensile strength of HDPE/$CaCO_3$/LDPE-g-MA composites decreased with increase in reaction temperature and $CaCO_3$ amount. These results were consistent with the study by Teixeira et al. [40]. The tensile strength of the composites in relation to the amount of LDPE-g-MA is given in Fig. 2. This was obtained from varying the amount of LDPE-g-MA for HCLM1 and HCLM7, which showed high tensile strength, as shown in Fig. 1. For both samples, the highest tensile strength was achieved when the LDPE-g-MA mass fraction was 16.68%. These results indicate that less LDPE-g-MA is inefficient as a compatibilizer, while more LDPE-g-MA fails to enhance the tensile strength.

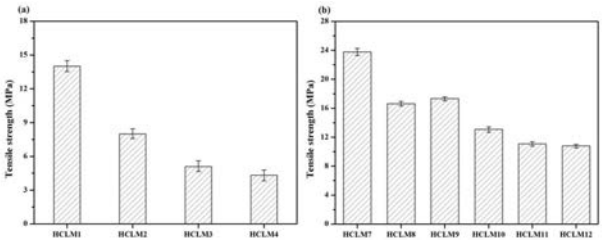

Fig. 1. Tensile strength of composites at various temperatures.

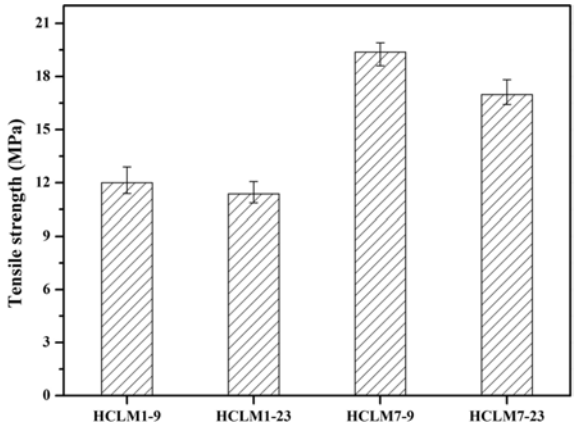

Fig. 2. Tensile strength of composites in relation to the amount of LDPE-g-MA.

The above results indicate that the reaction temperature and the amount of LDPE-g-MA play important roles in improving the tensile strength of pure HDPE matrix and $CaCO_3$. The composites prepared at appropriate temperatures can achieve higher tensile strength due to stronger reactions, since there is no decrease in the molecular weight of the polymer matrix. The tensile strength can be enhanced through adequate dispersion of inorganic fillers, accompanied by a specific amount of compatibilizer.

XRD analysis

The XRD patterns for all samples in relation to reaction temperature and LDPE-g-MA amount in Figs. 3 and 4, respectively, show peaks unique to $CaCO_3$ and HDPE with the dispersion of $CaCO_3$. No peaks were found for new crystal planes related to HDPE/$CaCO_3$/LDPE-g-MA composites. The reaction temperature and the amount of LDPE-g-MA did not have any significant influence on the crystal structure of $CaCO_3$ particles [2]. In addition, there was no substantial change in the *d*-spacing of any of the samples with increase in temperature, and the results are presented in Table 3. Table 4 shows that the *d*-spacing in relation to the amount of LDPE-g-MA also remained almost the same. These results indicate that the crystal structure of $CaCO_3$ particles is not significantly influenced by temperature, or by the amount of LDPE-g-MA.

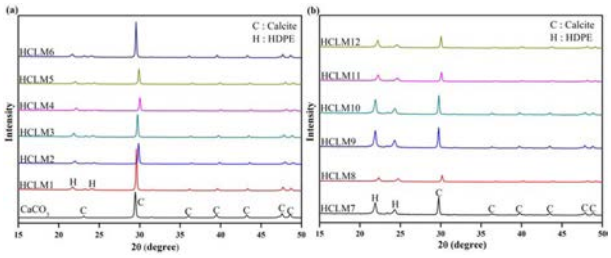

Fig. 3. XRD patterns in relation to the reaction temperature of the HDPE/$CaCO_3$/LDPE-g-MA composites.

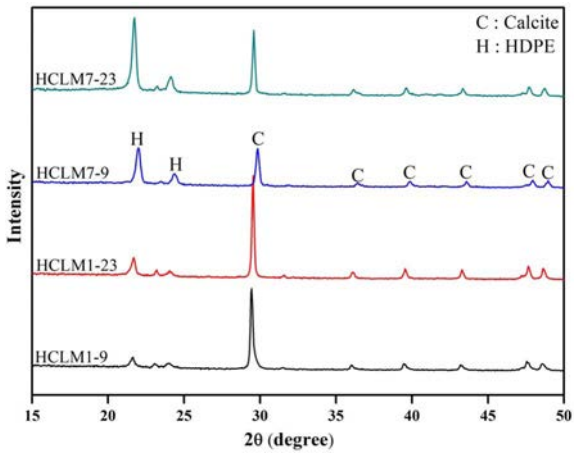

Fig. 4. XRD patterns in relation to the amount of LDPE-g-MA of the HDPE/CaCO3/LDPE-g-MA composites.

Table 3. Pattern positions in relation to the reaction temperature of the HDPE/$CaCO_3$//LDPE-g-MA composites.

Sample name	Angle (2θ)	*d*-spacing (nm)	hkl
HDPE	22.55	0.394	(110)
$CaCO_3$	29.45	0.303	(104)
HCLM1	21.7	0.409	(110)
	29.6	0.302	(104)
HCLM2	22	0.404	(110)
	29.85	0.299	(104)
HCLM3	21.85	0.406	(110)
	29.75	0.300	(104)
HCLM4	22.15	0.401	(110)
	30.05	0.297	(104)
HCLM5	22.05	0.403	(110)
	29.9	0.299	(104)
HCLM6	21.7	0.409	(110)
	29.55	0.302	(104)
HCLM7	21.9	0.406	(110)
	29.75	0.300	(104)
HCLM8	22.35	0.397	(110)
	30.2	2.957	(104)
HCLM9	21.9	0.406	(110)
	29.75	0.300	(104)
HCLM10	21.95	0.405	(110)
	29.75	0.300	(104)
HCLM11	22.25	0.399	(110)
	30.1	0.297	(104)
HCLM12	22.2	0.400	(110)
	30.05	0.297	(104)

Table 4. Pattern positions in relation to the amount of LDPE-g-MA of the HDPE/$CaCO_3$/LDPE-g-MA composites.

Sample name	Angle (2θ)	*d*-spacing (nm)	hkl
HCLM1-9	21.65	0.410	(110)
	29.45	0.303	(104)
HCLM1-23	21.70	0.409	(110)
	29.55	0.302	(104)
HCLM7-9	22.00	0.404	(110)
	29.85	0.299	(104)
HCLM7-23	21.75	0.408	(110)
	29.6	0.302	(104)

Physical reactions between HDPE and $CaCO_3$ do not generate new crystal structures, but helps to maintain the material properties. In other words, rather than generating new crystal structures, the LDPE-g-MA as a compatibilizer contributes to the dispersion of $CaCO_3$ particles in the HDPE matrix.

TGA analysis

The TGA curves of the pure HDPE and HDPE/$CaCO_3$/LDPE-g-MA composites in relation to the reaction temperature in Fig. 5. Table 5 presents the

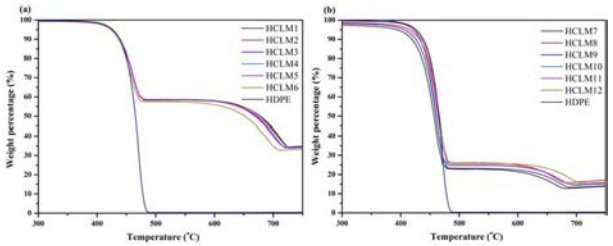

Fig. 5. TGA curves in relation to the reaction temperature of the HDPE/$CaCO_3$/LDPE-g-MA composites and pure HDPE.

Table 5. Evaluation of the thermal stability of the HDPE/$CaCO_3$/LDPE-g-MA composites in relation to the reaction temperature.

Sample name	$T_{25\%}$ (°C)	$T_{50\%}$ (°C)	$T_{60\%}$ (°C)	$T_{70\%}$ (°C)	$T_{80\%}$ (°C)	T_e (°C)
HDPE	453.98	465.20	468.45	471.25	474.09	485.29
HCLM1	457.66	677.48	–	–	–	727.50
HCLM2	457.42	673.25	–	–	–	727.50
HCLM3	456.95	669.26	–	–	–	719.75
HCLM4	457.19	676.54	–	–	–	727.50
HCLM5	456.95	670.67	–	–	–	719.75
HCLM6	454.14	651.17	–	–	–	712.00
HCLM7	438.40	456.72	462.59	468.23	619.00	696.50
HCLM8	447.09	464.23	470.11	475.74	650.00	681.00
HCLM9	444.98	460.01	465.17	470.58	634.50	688.75
HCLM10	446.86	460.95	465.88	471.05	650.00	696.50
HCLM11	450.14	464.7	470.34	475.98	650.00	696.50
HCLM12	452.96	466.35	471.75	477.15	673.25	704.25

stability results for temperature at a 25% weight loss ($T_{25\%}$), temperature at a 50% weight loss ($T_{50\%}$), and the finishing temperature (T_e). This table shows that the samples with higher amounts of $CaCO_3$ exhibit higher thermal stability than pure HDPE from $T_{25\%}$ and better stability in all areas. The samples in Table 5 with less amounts of $CaCO_3$ gradually attained temperatures higher than that of pure HDPE, and all samples were found to be more stable than pure HDPE at $T_{80\%}$. The thermal stability of the HDPE/$CaCO_3$/LDPE-g-MA composite did not differ in relation to T_e. The samples with less amounts of $CaCO_3$, from HCLM7 to HCLM12, had lower T_e than those from HCLM1 to HCLM6. These results are presumed to be the influence of the $CaCO_3$ fraction, and interactions between $CaCO_3$ and the HDPE matrix, and are also consistent with the tensile strength data. Fig. 6 shows the TGA curves in relation to the amount of LDPE-g-MA. Table 6, which is an assessment of thermal stability, shows that samples containing more $CaCO_3$ have a higher T_e. A comparison of HCLM1-9, HCLM1 and HCLM1-23 revealed high T_e for all samples except HCLM1-23 in Table 5 and 6. HCLM7 had the highest T_e compared to HCLM7-9 and HCLM7-23, indicating that high T_e can be attained at specific amounts of LDPE-g-MA. The composites showed no difference in T_e in relation to the reaction temperature but were more likely to undergo degradation

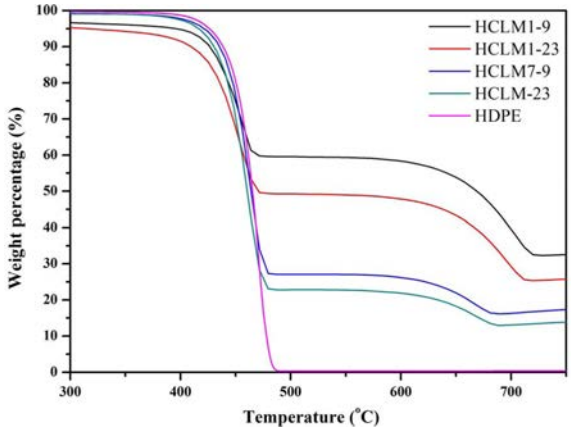

Fig. 6. TGA curves in relation to the amount of LDPE-g-MA of the HDPE/CaCO3/LDPE-g-MA composites and pure HDPE.

Table 6. Evaluation of the thermal stability of the HDPE/$CaCO_3$/LDPE-g-MA composites in relation to the amount of LDPE-g-MA.

Sample name	$T_{25\%}$ (°C)	$T_{50\%}$ (°C)	$T_{60\%}$ (°C)	$T_{70\%}$ (°C)	$T_{80\%}$ (°C)	T_e (°C)
HCLM1-9	449.75	669.41	699.16	–	–	727.50
HCLM1-23	442.39	470.97	666.20	–	–	719.75
HCLM7-9	451.08	463.77	468.93	476.45	661.19	688.75
HCLM7-23	446.15	460.71	465.64	470.65	634.19	688.75

at high temperatures than pure HDPE. Higher T_e was observed in samples containing relatively higher amounts of $CaCO_3$, and could be obtained at specific amounts of LDPE-g-MA. When the composites undergo thermal degradation, $CaCO_3$ serves as a heat barrier [2]. In addition, the HDPE/$CaCO_3$/LDPE-g-MA composites had enhanced thermal stability over the $CaCO_3$ nano-composites [25] used in past research. This is because LDPE-g-MA facilitates the dispersion of $CaCO_3$ in the HDPE matrix. In order to achieve high thermal stability, the focus should be on improving the dispersion of $CaCO_3$, rather than the particle size.

DSC analysis

The DSC curves in relation to reaction temperature of pure HDPE and HDPE/$CaCO_3$/LDPE-g-MA composites at a cooling rate of 5 °C/min in Fig. 7. These curves shifted vertically, and all composites had similar

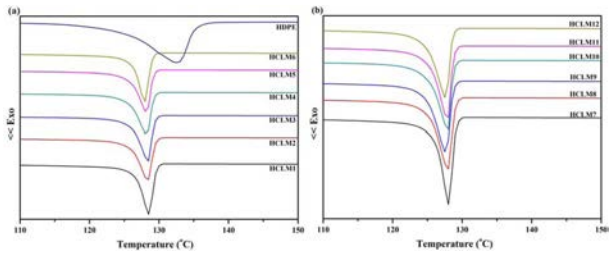

Fig. 7. DSC curves in relation to the reaction temperature of the HDPE/$CaCO_3$/LDPE-g-MA composites and pure HDPE.

Table 7. DSC analysis of the HDPE/$CaCO_3$/LDPE-g-MA composites in relation to the reaction temperature.

Sample name	T_f (°C)	T_c (°C)	T_o (°C)	ΔH_c (J/g)	X_c (%)	ΔS_c (J/g·°C)
HCLM1	122.14	127.99	132.07	72.19	59.11	0.564
HCLM2	121.07	127.63	131.91	71.12	58.24	0.557
HCLM3	124.45	127.8	131.81	70.69	57.88	0.553
HCLM4	121.32	127.63	131.7	70.55	57.77	0.552
HCLM5	120.58	127.59	131.64	69.32	56.76	0.543
HCLM6	120.58	126.84	130.96	67.84	55.55	0.534
HCLM7	127.7	128.19	132.35	179.5	81.68	1.400
HCLM8	125.69	128.15	132.52	174.2	79.27	1.359
HCLM9	125.2	127.85	131.94	176.1	80.14	1.377
HCLM10	122.99	128.11	131.94	178.3	81.14	1.391
HCLM11	126.19	128.05	131.94	173.6	78.99	1.355
HCLM12	124.96	127.82	131.69	174.4	79.36	1.364

crystallization peaks. Table 7 presents the crystallization onset temperature (T_o), crystallization temperature (T_c), crystallization finishing temperature (T_f), and crystallinity (X_c) of the composites. None of the composites showed any significant difference in crystallization temperature, but their melting enthalpy and X_c using the Eq. (2) decreased with increase in reaction temperature. In other words, the properties unique to HDPE deteriorate as the temperature increases. In addition, the decrease in X_c using the Eq. (2) of the composites is known to relate to conformational change. The ΔS_c by Eq. (3) of all the composites decreased with an increase in temperature. This means that the addition of $CaCO_3$ results in less space for macromolecules in the composites [35, 41]. The composites containing higher amounts of $CaCO_3$ were found to have lower ΔS_c. $CaCO_3$ lowers the mobility of

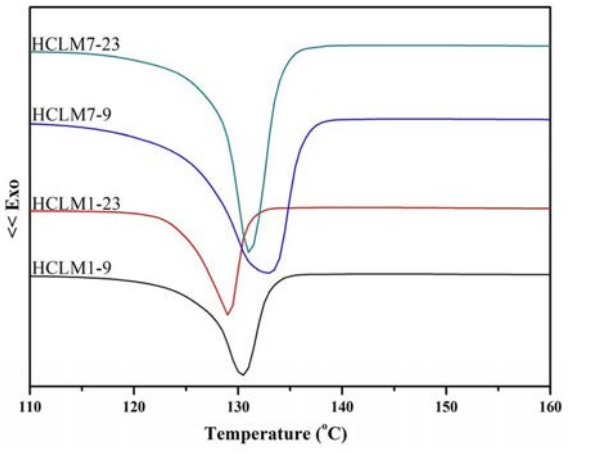

Fig. 8. DSC curves in relation to the amount of LDPE-g-MA of the HDPE/$CaCO_3$/LDPE-g-MA composites and pure HDPE.

Table 8. DSC analysis of the HDPE/$CaCO_3$/LDPE-g-MA composites in relation to the amount of LDPE-g-MA.

Sample name	T_f (°C)	T_c (°C)	T_o (°C)	ΔH_c (J/g)	X_c (%)	ΔS_c (J/g·°C)
HCLM1-9	126.88	132.9	139.18	80.88	76.68	0.6085
HCLM1-23	125	129.09	136.97	66.16	49.09	0.5125
HCLM7-9	125.72	132.94	144	203.3	95.05	1.5292
HCLM7-23	127.98	131.18	141.93	162.3	71.94	1.2372

reduced space for macromolecules caused by $CaCO_3$ can be seen as the result of LDPE-g-MA acting as a compatibilizer.

Non-isothermal crystallization behavior

Fig. 9 and Table 9 show DSC data obtained under

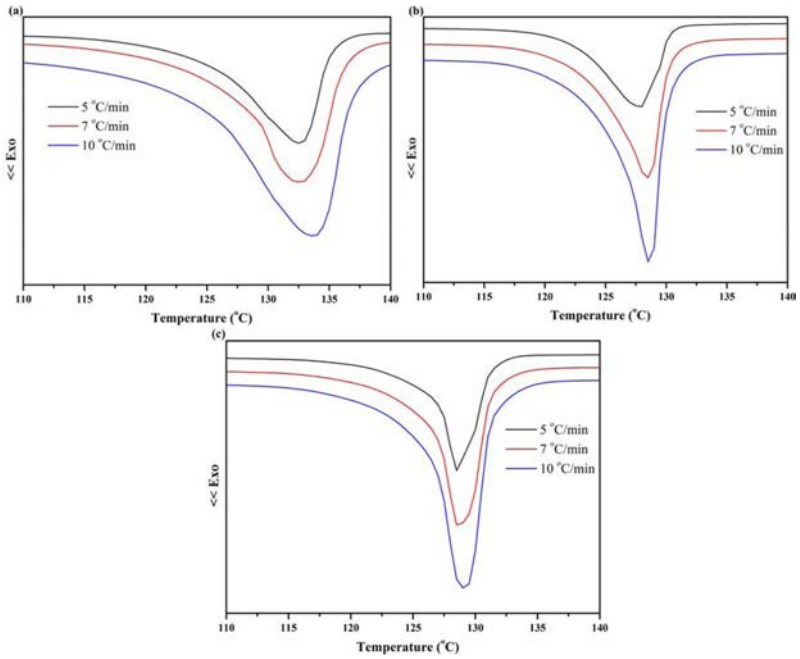

Fig. 9. DSC curves at various cooling rates: (a) pure HDPE, (b) HCLM1, and (c) HCLM7.

Table 9. The crystallization temperature and half crystallization time at various cooling rates for pure HDPE, HCLM1, and HCLM7.

Sample name	α (°C/min)	T_c (°C)	$t_{1/2}$ (min)
HDPE	5	132.45	2.02
	7	133.04	1.35
	10	133.67	0.92
HCLM1	5	127.99	2.74
	7	128.33	2.04
	10	128.72	1.28
HCLM7	5	128.19	2.44
	7	128.53	1.91
	10	128.96	1.19

various cooling rates. The crystallization temperature of the composites was lower than that of pure HDPE. To examine the non-isothermal crystallization behavior, the crystallization kinetic of pure HDPE was compared to that of the composites.

Fig. 10 presents the relative crystallinity for pure HDPE and composites derived from Eq. (4) at the given cooling rate. The plots of T in relation to X_T for pure HDPE and composites were similar to a sigmoid. This can be attributed to the lag effect of the cooling rate in the crystallization process. Fig. 11 converts the X-axis of Fig. 10 into crystallization time using Eq. (5). At a faster cooling rate, a shorter time is required for complete crystallization. When X_t reaches 50%, this time is known as the half crystallization time ($t_{1/2}$), and it is widely used to express the crystallization rate. The $t_{1/2}$ decreased with increase in the cooling rate. At the given cooling rate, the $t_{1/2}$ values of the composites were higher than that of pure HDPE, and increased with the $CaCO_3$ amount. We presumed that instead of acting as a nucleating agent, the $CaCO_3$ in composites suppressed the crystal growth, thus confirming the absence of substantial change in crystal structure of the composites, as observed in XRD. Based on the above results, a lower crystallization temperature was expected with the suppressed crystal growth of $CaCO_3$, and a slower crystallization rate with the increase in $t_{1/2}$. To verify these results, we employed the Avrami model to analyze the non-isothermal crystallization kinetics of HCLM1, HCLM7, and pure HDPE.

Non-isothermal crystallization kinetic and activation energy

Research on non-isothermal crystallization behavior is being conducted under conditions very similar to the real-world process. The most widely used Jeziorny's method has been derived from the Avrami model.

Fig. 12 was derived from Eq. (6). The n and Z_t values were obtained from the gradient and intercept. According to Jeziorny, the influence of the cooling rate should be considered for Z_t. Table 10 presents the results obtained from the Avrami model and Jeziorny's method. The Avrami exponent n is influenced by the nucleation shape and secondary crystallization. At the given cooling rate, the n values of HDPE/$CaCO_3$/LDPE-g-MA composites were slightly higher than that of pure HDPE. The repressed crystal growth in the crystallization kinetic of the composites prevented $CaCO_3$ from acting efficiently as a nucleating agent. The Z_c values of the composites were slightly lower than pure HDPE, and decreased with increasing amounts of $CaCO_3$. The dispersal $CaCO_3$ particles due to the addition of

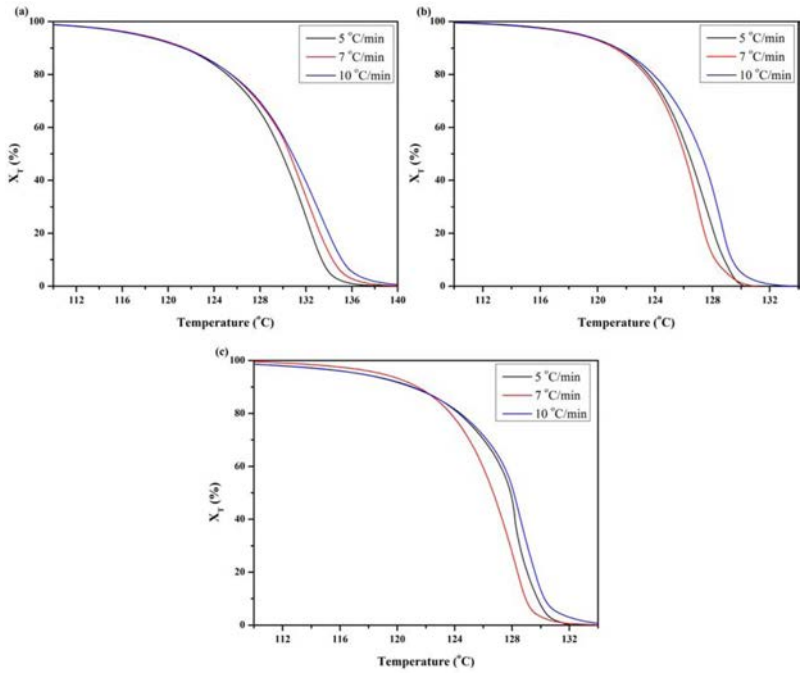

Fig. 10. Relative crystallinity with various temperatures at various cooling rates: (a) pure HDPE, (b) HCLM1, and (c) HCLM7.

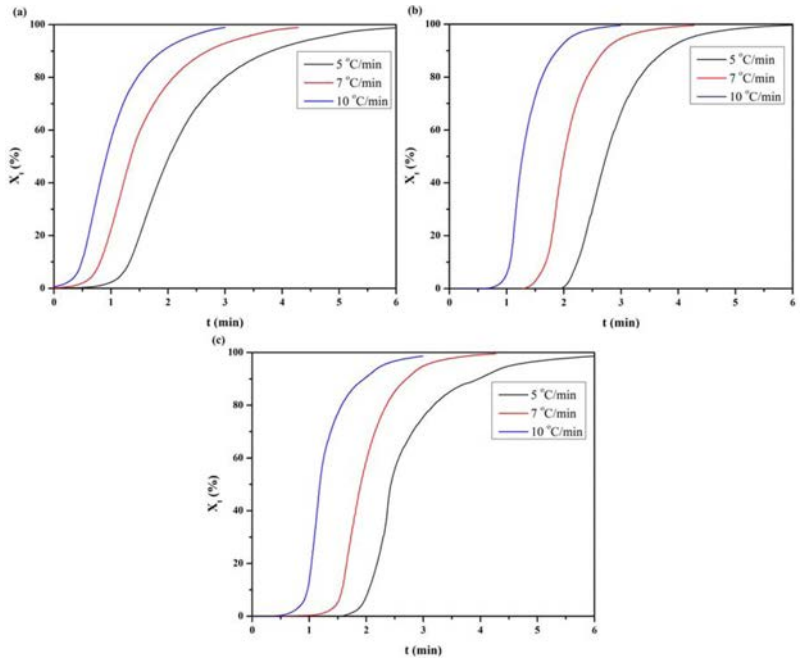

Fig. 11. Relative crystallinity in relation to crystallization time at various cooling rates: (a) pure HDPE, (b) HCLM1, and (c) HCLM7.

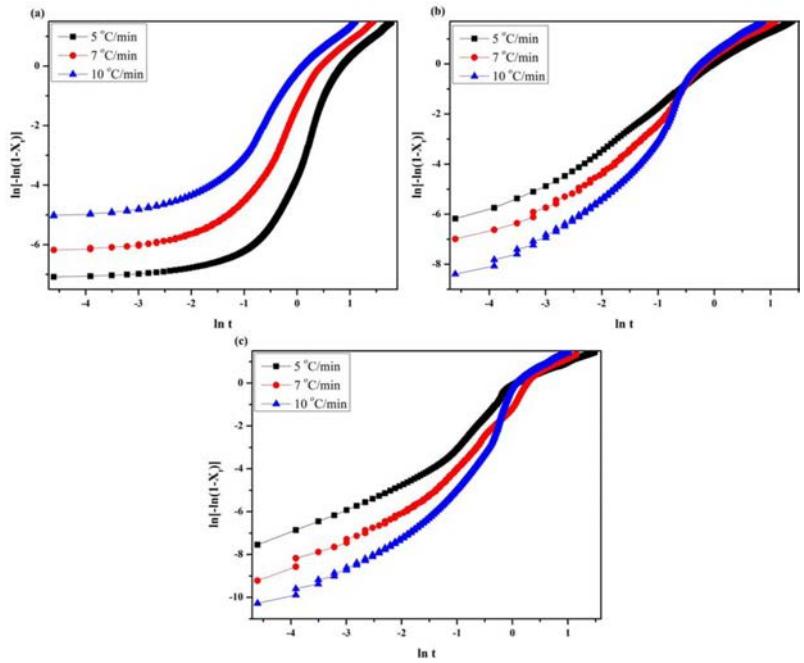

Fig. 12. Non-isothermal crystallization parameters derived from the Avrami model and Jeziorny's method: (a) pure HDPE, (b) HCLM1, and (c) HCLM7.

LDPE-g-MA prevented them from functioning as a stable nucleating agent, thus slowing the rate of crystallization. This is consistent with the decrease in crystallization temperature. The average Z_c of HCLM7, which contains relatively less $CaCO_3$, was not significantly different from that of pure HDPE. The Z_c value can be increased with $CaCO_3$ acting as a stable nucleating agent when the $CaCO_3$ is added in small amounts.

Huang et al. [42] observed the rate of crystallization after the addition of PE-g-MA to nano-sized $CaCO_3$ and HDPE. The Z_c values were not that different from HCLM1 and 7, and the latter had a faster Z_c. Deshmukh et al. [43] examined the crystallization temperature and rate for a mixture of polybutylene terephthalate (PBT) and nano-$CaCO_3$. PBT composites (PBT/nano-$CaCO_3$) containing nano-$CaCO_3$ had a higher crystallization temperature and faster rate than pure PBT. Since the crystallization temperature of PBT was higher than HDPE, the crystallization temperature of PBT/nano-

Table 10. Non-isothermal crystallization parameters by the Avrami model, Jeziorny's method, and activation energy using the Kissinger method.

Sample name	α (°C/min)	n	$\ln Z_t$	Z_c	R^2	E_a (kJ/mol)	R^2
HDPE	5	2.43	-2.63	1.69	0.91	786.21	0.99
	7	2.09	-1.38	1.22	0.94		
	10	1.77	-0.40	1.04	0.94		
HCLM1	5	1.47	-0.16	1.03	0.99	1278.22	0.99
	7	1.91	-0.07	1.01	0.97		
	10	2.41	0.023	0.99	0.96		
HCLM7	5	1.71	-0.72	1.16	0.96	1210.54	0.99
	7	2.35	-1.07	1.17	0.97		
	10	2.91	-1.03	1.11	0.95		

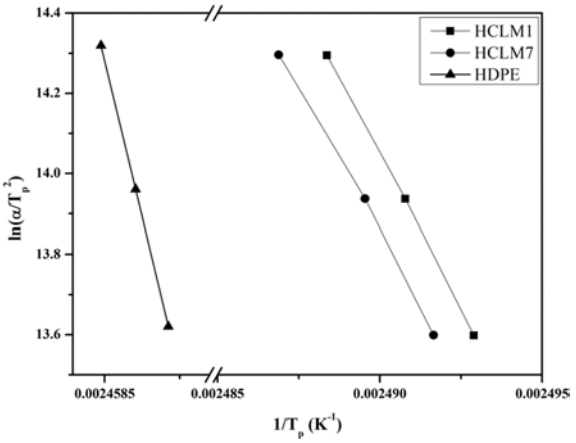

Fig. 13. Plots of pure HDPE and composites based on the Kissinger method.

$CaCO_3$ composites was also higher. Moreover, the Z_c values of PBT/nano-$CaCO_3$ were not noticeably different from that of HCLM7. From this, we can presume that the rate of crystallization is not significantly influenced by the particle size of $CaCO_3$.

The activation energy (E_a) was calculated using the Kissinger method of Eq. (8). The plots of $1/T_c$ against $\ln(\alpha/T_c^2)$ are shown in Fig. 13, while Table 10 shows the E_a of pure HDPE and the composites derived from the gradient of Eq. (8). The E_a of the composites was higher than that of pure HDPE, and increased with increasing amount of $CaCO_3$. This is similar to the increase in E_a due to PE-g-MA facilitating the dispersion of inorganic fillers [44-46]. A closer examination of the dispersion of $CaCO_3$ shows that the carboxylate-inorganic component introduces a carboxylic group to the surface of the inorganic filler with the addition of maleic anhydride of PE-g-MA [47]. The $CaCO_3$ in composites containing LDPE-g-MA exists as "carboxylate-$CaCO_3$", and the hydroxyl group of "carboxylate-$CaCO_3$" forms an ester bond with the carbonyl group of the LDPE-g-MA anhydride [48], thus facilitating $CaCO_3$ dispersion. While the enhanced interactions with the polymer support $CaCO_3$ dispersion, the carboxylate group is known to suppress the crystal growth of $CaCO_3$ [49-51]. In this connection, the future goal of this research is not only to support the $CaCO_3$ being well-dispersed, but also to improve the rate of crystallization, with $CaCO_3$ crystal growth acting as a nucleating agent.

Conclusions

This study investigated the properties of HDPE/$CaCO_3$/LDPE-g-MA composites in relation to reaction temperature and the amount of LDPE-g-MA. When melt mixing was performed at high temperatures, the tensile strength of the composites decreased with increase in temperature, because thermal degradation led to deterioration in the HDPE matrix functions. The higher tensile strength was achieved using samples containing more HDPE, and the highest tensile strength was observed in HCLM1 and HCLM7, which had 16.68% of LDPE-g-MA. This was because the temperature and the amount of LDPE-g-MA play significant roles in determining the tensile strength of composites. Both adequate temperature and amount of LDPE-g-MA were thus necessary to enhance the tensile strength. Meanwhile, the crystal structure of the composites remained unaffected by the temperature and the amount of LDPE-g-MA. TGA revealed degradation in the thermal stability of the composites with the addition of $CaCO_3$ at high temperatures, compared to pure HDPE. A higher T_e was observed in samples containing relatively higher amounts of $CaCO_3$, and was obtained at specific amounts of LDPE-g-MA. Melting enthalpy, X_c and ΔS_c decreased with increase in temperature and the amount of LDPE-g-MA. These results indicated that the addition of $CaCO_3$ to composites reduces the space for macromolecules.

DSC was performed to examine the non-isothermal crystallization kinetic of the composites. The rate of crystallization increased with decreasing amounts of $CaCO_3$, which suggests that small amounts of $CaCO_3$ can serve as a stable nucleating agent. The composites comprised of "carboxylate-$CaCO_3$" exhibited higher activation energies than pure HDPE, due to the enhanced affinity with polymers, but repressed crystal growth occurring in the presence of the carboxylate group was an issue to be resolved. The interactions between the filler and the polymer matrix of composites were influenced by the reaction temperature and the LDPE-g-MA amount. Specific amounts of $CaCO_3$, serving as a stable nucleating agent, are expected to increase the rate of crystallization. Considering the function of $CaCO_3$ as a stable nucleating agent, the focus should be on the dispersion and interaction of $CaCO_3$ with the polymer, rather than on the particle size. This composite may find application as a potential material for automotive

weight reduction, and filament of 3D printing.

Acknowledgments

The present research has been conducted by the Korea Institute of Energy Technology Evaluation and Planning (Grant No. 2013T100100021).

References

1. G. Matsuba, S. Sakamoto, Y. Ogino, K. Nishida, T. Kanaya, Macromolecules 40[20] (2007) 7270-7275.
2. Y. Ahn, J.H. Jeon, J.H. Park, T. Thenepalli, J.W. Ahn, C. Han, Korean J. Chem. Eng. 33[11] (2016) 3258-3266.
3. J.Z. Liang, B. Li, J.Q. Ruan, Polym. Test. 42 (2015) 185-191.
4. C.M. Chan, J. Wu, J.X. Li, Y.K. Cheung, Polymer 43[10] (2002) 2981-2992.
5. M. Tanniru, R.D.K. Misra, Mater. Sci. Eng. A Struct. Mater. 405[1-2] (2005) 178-193.
6. M. Tanniru, R.D.K. Misra, Mater. Sci. Eng. A Struct. Mater. 424[1-2] (2006) 53-70.
7. L. Dong, L. Yang, Y. Wang, M. Han, J. Cryst. Growth. 343[1] (2012) 86-94.
8. H. Ghasemi, A. Mirzadeh, P.J. Bates, M.R. Kamal, Polym. Test. 42 (2015) 69-78.
9. J. Hu, Z.W. Wang, S.M. Yan, X.Q. Gao, C. Deng, J. Zhang, K. Shen, Polym. Plast. Technol. 51[11] (2012) 1127-1132.
10. W.Y. Wang, X.F. Zeng, G.Q. Wang, J.F. Chen, J. Appl. Polym. Sci. 106[3] (2007) 1932-1938.
11. T. Kato, Adv. Mater. 12[20] (2000) 1543-1546.
12. K. Haraguchi, J. Ning, G. Li, Eur. Polym. J. 68 (2015) 630-640.
13. H. Ebadi-Dehaghani, M. Barikani, H.A. Khonakdar, S.H. Jafari, U. Wagenknecht, G. Heinrich, Polym. Test. 45 (2015) 139-151.
14. F.A. Santos, M.I.B. Tavares, Polym. Test. 47 (2015) 92-100.
15. L. Verdolotti, M. Lavorgna, R. Lamanna, E.D. Maio, S. Iannace, Polymer 56 (2015) 20-28.
16. R.S. Hadal, R.D.K. Misra, Mater. Sci. Eng. A Struct. Mater. 374[1-2] (2004) 374-389.
17. G. Siqueira, K. Oksman, S.K. Tadokoro, A.P. Mathew, Compos. Sci. Technol. 123 (2016) 49-56.
18. D. Liu, Q. Bian, Y. Li, Y. Wang, A. Xiang, H. Tian, Compos. Sci. Technol. 129 (2016) 146-152.
19. L. Zuo, W. Fan, Y. Zhang, L. Zhang, W. Gao, Y. Huang, T. Liu, Compos. Sci. Technol. 139 (2017) 57-63.
20. A. Mirzadeh, H. Ghasemi, M.R. Kamal, P.J. Bates, Int. Polym. Proc. 29[1] (2014) 4-12.
21. W.Y. Wang, X.F. Zeng, G.Q. Wang, J.F. Chen, J. Appl. Polym. Sci. 106[3] (2007) 1932-1938.
22. J.Z. Liang, J. Appl. Polym. Sci. 104[3] (2007) 1697-1701.
23. M.A. Osman, A. Atallah, U.W. Suter, Polymer 45[4] (2004) 1177-1183.
24. A. Lazzeri, S.M. Zebarjad, M. Pracella, K. Cavalier, R. Rosa, Polymer 46[3] (2005) 827-844.
25. S. Sahebian, S.M. Zebarjad, S.A. Sajjadi, J. Thermoplast. Compos. Mater. 23[5] (2010) 583-596.
26. A. Chafidz, I. Ail, M.E.A. Mohsin, R. Elleithy, S. Al-Zahrani, J. Polym. Res. 19 (2012) 9860-9876.
27. H.U. Zaman, M.A. Khan, R.A. Khan, M. Dalour Hossen Beg, J. Thermoplast. Compos. Mater., 27[12] (2014) 1701-1710.
28. J.Z. Liang, F. Wang, Polym. Bull., 72[4] (2015) 915-929.
29. A. Martinez-Garcia, A. Sanchez-Reche, C.M. Cepeda-Jimenez, and J.M. Martin-Martinez, Macromol. Symp. 221[1] (2005) 23-32.
30. G. Wang, X.Y. Chen, R. Huang, J. Mater. Sci. Lett. 21[13] (2002) 985-986.
31. X.L. Xie, Q.X. Liu, R.K.Y. Li, X.P. Zhou, Q.X. Zhang, Z.Z. Yu, Y.W. Mai, Polymer 45[19] (2004) 6665-6673.
32. R. Chen, W. Zou, H. Zhang, G. Zhang, Z. Yang, G. Jin, J. Qu, Polym. Test. 42 (2015) 160-167.
33. Y.S. Thio, A.S. Argon, R.E. Cohen, M. Weinberg, Polymer 43[13] (2002) 3661-3674.
34. B. Wunderlich, M. Dole, J. Polym. Sci. Pol. Chem. 24[106] (1957) 201-213.
35. A. Chafidz, M.A. Ail, R. Elleithy, J. Mater. Sci. 46 (2011) 6075-6086.
36. M. Avrami, J. Chem. Phys. 7[12] (1939) 1103-1112.
37. A. Jeziorny, Polymer 19[10] (1978) 1142-1144.
38. H.E. Kissinger, Anal. Chem. 29[11] (1957) 1702-1706.
39. Y. Wang, X. Cao, L. Zhang, Macromol. Biosci. 6[7] (2006) 524-531.
40. S.C.S. Teixeira, M.M. Moreira, A.P. Lima, L.S. Santos, B.M. da Rocha, E.S. de Lima, R.A.A.F. da Costa, A.L.N. da Silva, M.C.G. Rocha, F.M.B. Countinho, J. Appl. Polym. Sci. 101[4] (2006) 2559-2564.
41. R.H. Elleithy, I. Ali, M.A. Ali, S.M. Al-Zahrani, J. Appl. Polym. Sci. 117[4] (2010) 2413-2421.
42. J.W. Huang, Y.L. Wen, C.C. Kang, W.J. Tseng, M.Y. Yeh, Polym. Eng. Sci. 48[7] (2008) 1268-1278.
43. G.S. Deshmukh, D.R. Peshwe, S.U. Pathak, J.D. Ekhe, Thermochim. Acta 606 (2015) 66-76.
44. J. Li, C. Zhou, W. Gang, Polym. Test. 22[2] (2003) 217-223.
45. Y.C. Kim, S.J. Lee, J.C. Kim, H. Cho, Polym. J. 37 (2005) 206-213.
46. M.J. Solomon, A.S. Almusallam, K.F. Seefeld, S. Somwangthanaroj, P. Varadan, Macromolecules 34[6] (2001) 1864-1872.
47. P.A. Ciullo, "Industrial Minerals and Their Uses: A Handbook and Formulary" (Noyes Publications, 1996) p. 86-92.
48. R.M. Rowell, J. Polym. Environ. 15[4] (2007) 229-235.
49. S. Zhang, K.E. Gonsalves, Langmuir 14[23] (1998) 6761-6766.
50. S. Boggavarapu, J. Chang, P. Calvert, Mater. Sci. Eng. C 11[1] (2000) 47-49.
51. K. Naka, Y. Tanaka, Y. Chujo, Y. Ito, Chem. Commun. 19 (1999) 1931-1932.